Soil texture approach to drought risk management using long-term ERA5 dataset and geospatial techniques in a semi-arid ecosystem

Firas K. Aljanabi [1]*, Mert Dedeoğlu [2]

[1,2] Selcuk University, Faculty of Agriculture, Department of Soil Science and Plant Nutrition, Alaaddin Keykubat Campus, 42130, Konya, Turkey

* Corresponding author: PhD in Soil Science, Firas Aljanabi, firask.aljanabi@gmail.com, ORCID ID: https://orcid.org/0000-0002-5122-3699

Abstract

Assessing soil moisture is an essential measure of aridity and has become a significant field of study for monitoring dry conditions, particularly following recent years' climate change developments. This article aims to evaluate three drought indices, the Perpendicular Drought Index (PDI), Soil Moisture Monitoring Index (SMMI), and Modified Soil Moisture Monitoring Index (MSMMI), within the Gozlu agricultural enterprise located in Konya Province, Turkey, which is characterized by a semi-arid ecosystem. It also tests the correlation between long-term precipitation data and the selected drought indices while exploring the relationship between the most correlated drought index with long-term precipitation spatial data on the one hand and the spatial distribution of soil texture on the other. This study was conducted in two stages. In the first stage, we used Sentinel-2 data to derive drought indices and the ERA5 dataset to calculate the long-term mean total monthly precipitation (LT-MTMP). We then performed a Pearson correlation coefficient analysis between these two data sets. In the second stage, we collected 100 composite samples from a 0-30 cm depth in the study area to determine the soil texture using the hydrometer method based on the USDA classification system. We then created an interpolated map of soil texture classes. Subsequently, the soil texture map was combined with the drought index map, which showed the highest correlation with LT-MTMP by geospatial techniques to explain the relationship between the spatial distribution of soil texture and the drought index. The research findings indicate that the PDI index has the highest negative correlation coefficient (r = -0.69, P < 0.01) with LT-MTMP, meaning that a decrease in the drought index corresponds to an increase in precipitation spatially. On the other hand, the SMMI and MSMMI indices possess correlation coefficients of (r = -66, P < 0.01) and (r = -24, P < 0.05), respectively. Laboratory analysis revealed four distinct soil textures within the studied area: Sandy Loam (SL), Loam (L), Sandy Clay Loam (SCL) and Clay Loam (CL). This approach provides a deeper understanding of soil data behavior over several years when linked drought indices with long-term climate factors. Additionally, geo-statistical combination techniques enabled the interpretation of the relationship between the spatial distribution of soil moisture and soil texture, thus facilitating land management and providing a useful tool for drought management plans.

1. Introduction

Drought, a common natural phenomenon, significantly impacts societal and economic progression, contributes to various environmental issues, and leads to natural calamities such as alterations in surface water flow, decimation of agricultural output, and desertification (Mishra and Singh, 2010). Soil hydration is equally a fundamental requirement for crop cultivation and maturation. A lack of adequate water resources can impede crop growth, indirectly resulting in diminished crop yields (Quiring and Ganesh, 2010). Global temperatures have risen by approximately 0.74°C over the past century, leading to widespread and unexpected land degradation, particularly in mid-latitude, arid, and semi-arid regions worldwide (Jiang et al., 2017). Further-more, numerous research studies suggest that the extent of extremely arid land is anticipated to rise in the forthcoming years. This condition is expected to worsen especially during the summer season in continental regions (Zhang et al., 2019; Gümüş et al., 2023; Kimura et al., 2023). Given the prevailing climate change situation, the outcomes of such aridity tendencies might be disastrous. As such, it's of utmost importance to identify areas afflicted by drought, observe the severity of the drought, and assess its repercussions on agriculture, the environment, and economic conditions. This is vital for managing regional drought risk and formulating sustainable development strategies (Hao et al., 2012).

Based on a variety of remote sensing data, remote sensing technology is one of the best ways to monitor dryness across

large scale areas (Yue et al., 2021). A multitude of dryness indicators have been introduced, for instance: Temperature Condition Index (TCI) (Singh et al., 2003), Vegetation Condition Index (VCI) (Dutta et al., 2015), Temperature Vegetation Dryness Index (TVDI) (Liu et al., 2015), thermal inertia (Kang et al., 2017), indices derived from Near-Infrared (NIR) - Red space (Liu et al., 2013), and microwave techniques (Sawada, 2018). These dryness indices encompass visible wavelengths, NIR bands, microwave wavelengths, and thermal infrared bands. Spectral feature space-based methods are commonly used to assess dryness or conditions of soil moisture because of their clear biophysical implications and the simplicity of data acquisition and processing (Liu et al., 2021). Chen in his study (Chen et al., 2015) utilized the PDI and modified perpendicular drought index (MPDI) to evaluate the effectiveness of Gaofen-1 (GF-1) wide field of view (WFV) sensors in observing soil moisture in Wuhan city, suggested that the WFV sensor can be employed to evaluate the state of the soil water content. Zhang and Chen (2016) devised a satellite and in situ sensor collaborative reconstruction (SICR) approach to recover missing pixels impacted by clouds and employed the PDI and MPDI to assess the effectiveness of using the reconstructed GF-1 data for soil moisture inversion. In a study conducted by Liu et al. (2020), soil moisture was retrieved using the MSMMI and MPDI indices from Sentinel-2A images. The results showed that MSMMI could monitor soil moisture more accurately in bare soil areas, performing slightly better than synthetic aperture radar (SAR). The performances and differences of the PDI, SMMI, MPDI, and MSMMI indices were evaluated using field-measured soil moisture in an arid and semiarid region by (Yue et al., 2021). The study found that when utilizing Landsat-8 data, PDI and SMMI had comparable soil moisture evaluation capabilities that were superior to those of MPDI and MSMMI.

Jiang et al. (2020) used the Standardized Precipitation Evapotranspiration Index (SPEI) and the Normalized Difference Vegetation Index (NDVI) for the period 1982–2015 to investigate how soil characteristics affect to plant reaction to drought in a fragile environmental location. In another study conducted by Renne et al. (2019) on the effects of soil texture and seasonal precipitation on water distribution in soils with fine versus coarse textures in dry lands, the study concluded that coarse-textured soils facilitate water infiltration into deep soil layers and reduce evaporation from bare soil, creating a suitable environment for perennial plants with deep roots. Conversely, fine-textured soils retain water in the surface layers, making them more suitable for plants with shallow to medium roots.

By reviewing dryness indices that utilize the NIR–Red spectral space, along with relevant studies on this topic, we identified the main aims of our paper as follows:

(1) According to open access satellite data from Sentinel-2, the drought indices (PDI, SMMI, and MSMMI) were derived, which utilize the NIR-Red feature space, were utilized to analyse the variations in topsoil moisture at the Gozlu Agricultural Enterprise in Konya, Turkey;

(2) The link between drought indices (PDI, SMMI, and MSMMI) and long-term precipitation data for the period from 2019 to 2023 is investigated in this study;

(3) This paper focuses on combining the drought index that is most correlated to long-term precipitation data with the spatial distribution of soil texture classes using geospatial techniques;

(4) Manage the lands within the area of interest based on soil texture type and its moisture retention capacity.

2. Materials and methods

2.1. Study area

The Gozlu agricultural enterprise directorate in Konya/ Turkey, which is a branch of the general directorate of agricultural enterprises, has been chosen (Fig. 1). The province of Konya, home to the Gozlu agricultural enterprise, is subject to a climate that includes hot, dry summers and cold, rainy winters. Considering the two main climatic elements within Thornthwaite climate classification (temperature and precipitation) areas like Konya-Central, Karaman, Saraykoy, and Cihanbeyli are categorized under the semi-arid and primary Mesothermal climate (Abdikan et al., 2023). Rainfall generally increases in the southwestern and southern parts of the Konya province, with a diminishing trend as one goes north and east. The yearly average rainfall in Konya is approximately 326.1 mm, with May typically having the highest monthly average and August the lowest. The region's average annual temperature is around between 10.7°C and 25.3°C, with July being the hottest month and January the coldest (Özen et al., 2021). (Fig. 2) presents the mean monthly precipitation and temperature of Konya province for the period (1929–2023) (https://www.mgm.gov.tr).

The Gozlu agricultural enterprise is located in the Sarayönü district, roughly 78 km distant from the Konya city center. The area of study lies within the geographical coordinates of 38°45'00"–38°22'30" North latitude and 32°15'00"–32°37'30" East longitude. This enterprise spans a vast area of 28,829.7 hectares and exemplifies the continental (semi-arid) climate characteristics unique to the Anatolian Plateau. Most of the land in the study area is used for producing wheat, barley, and corn under a rainfed agriculture system. The region's Plains foundation is comprised of Paleozoic schists, Mesozoic limestones, and igneous masses. Overlying these geological bases are Neogene formations, which include limestone, clay, marl, and clayey sandy deposits. The topographical features pervade most of the enterprise's territory, which spans flat to semi-flat, slightly inclined, and rolling landscapes (ÇÜ and TİGEM, 1998).

2.2. Methods

In this case, we employed three drought indices (PDI, SMMI, and MSMMI), which are based on spatial features of moisture distribution in the NIR and Red spectral space. We selected the PDI and SMMI indices based on the timing of the experiment in September, a period when most agricultural fields are devoid of crops, which enhances the accuracy of these indices. In contrast, we chose the MSMMI index for its ability to estimate soil moisture in the presence of fractional vegetation cover, thereby achiev-
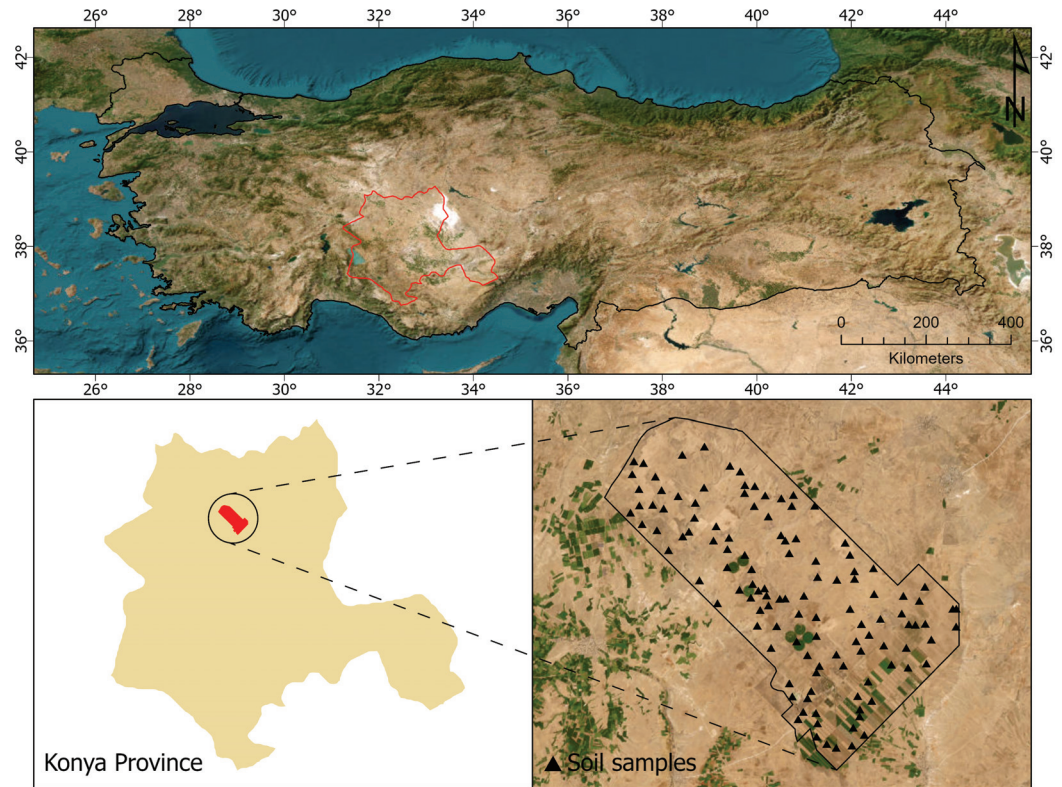
2

Fig. 1. Location of the study area and spatial distribution of soil samples
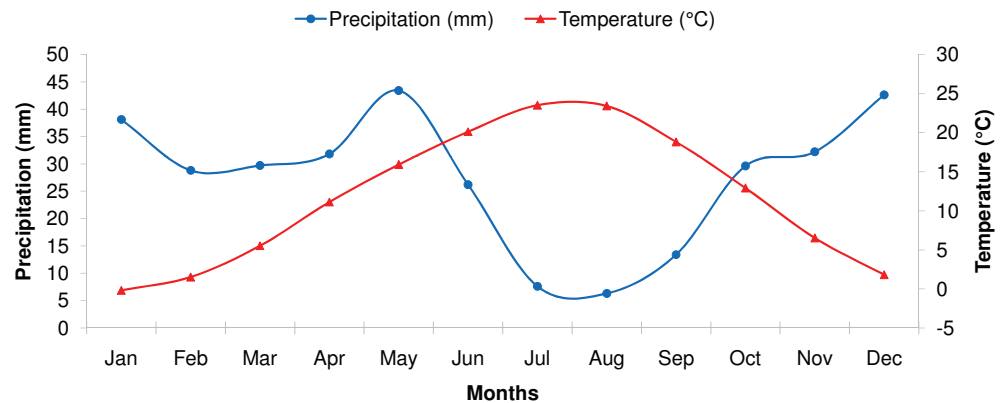

Fig. 2. Mean monthly precipitation and temperature of Konya province

ing greater accuracy in soil drought assessment. Through open-source remote sensing data, we utilized Sentinel-2 multispectral instrument (MSI) satellite data captured in September 2023. This was done in conjunction with collecting soil samples for soil texture analysis. We also derived the precipitation LT-MTMP from ERA5 data for five years, covering the period from 2019 to 2023, using the Google Earth Engine platform. We performed the satellite image processing chain and derived the drought indices using ArcGIS Pro software version (2.5). R-Studio software version (2024.04.1+748) was utilized to analyze the Pearson correlation coefficient (PCC), denoted as (r), is employed to quantify the linear dependence or similarity between the drought indices and LT-MTMP, can be calculated using the following equation:

$$r = \frac{\sum (x_i - \bar{x})(y_i - \bar{y})}{\sqrt{\sum (x_i - \bar{x})^2 \sum (y_i - \bar{y})^2}}$$

where x_i represents the sample values of LT-MTMP, $\bar{x}$ depicts the LT-MTMP mean values, y_i represents the sample values of the drought index, and $\bar{y}$ represents the mean values of the drought index. We carried out soil sampling according to four soil orders Entisol, Vertisol, Inceptisol, and Mollisol as identified in the soil survey report (ÇÜ and TİGEM, 1998). In total, we took one hundred (100) composite samples at a depth of 0 to 30 cm (Figure 1). We used a handheld global positioning system (GPS) to facilitate soil sampling. The soil was air-dried and passed through a 2.0 mm sieve. We determined the soil texture using the hydrometer method according to USDA system, as outlined in (Bouyoucos, 1951).

We created the soil texture interpolated map of the study area using the Inverse Distance Weighted (IDW) model through the Geostatistical Wizard within the ArcGIS Pro software environment. The IDW model estimates values at unsampled loca-

3

tions by averaging the values of nearby sample points, assigning weights that are inversely proportional to their distance from the prediction location (Kaya et al., 2022). The value a_j for a given location j is computed using the underlying IDW equation:

$$\hat{a}_j = \sum_{i=1}^{n} w_{i,j} \hat{a}_i$$

where a_i ($i = 1, ..., n$) represents the observed value at location i, and $w_{i,j}$ is the weight assigned to the data point at location i. $w_{i,j}$ is calculated using the following equation:

$$w_{i,j} = \frac{d_{i,j}^{-\alpha}}{\sum_{k=1}^{n} d_{i,j}^{-\alpha}}$$

where, $d_{i,j}$ represents the Euclidean distance between a data point located at position i and an unknown data point at position j; n denotes the total number of available data points; and α, a control parameter, represents the power. Increasing α amplifies the influence of nearby points, resulting in a more localized interpolation. We isolated each soil texture class as a separate raster and paired it with the drought index raster that demonstrated the strongest correlation with LT-MTMP. This process was carried out using geoprocessing tools within the ArcGIS Pro software environment to determine and quantify the levels of dryness within each soil texture class. Table 1 displays the five categories into which the levels of the drought index were categorized, with an interval of 0.2: very dryness class, dryness class, normal class, wet class, and very wet class (Liu and Yue, 2018; Yue et al., 2021).

Table 1
Soil dryness levels

Dryness levels	Scale
Very wet	(0.0 to 0.2)
Wet	(0.2 to 0.4)
Normal	(0.4 to 0.6)
Dryness	(0.6 to 0.8)
Very dryness	(0.8 to 1.0)

To verify the results more deeply, we compared the NDVI for the last three years (2021, 2022, and 2023) with the study results because the geographical distribution of vegetation affects the carbon cycle in the soil (Zhu et al., 2022), thereby increasing the soil's ability to retain water (Jiang et al., 2020). These operations were conducted using the tools provided by the geo-statistical Analyst within the ArcGIS Pro software environment. (Fig. 3) presents the flowchart of the methodology employed in this study.

2.2. Drought indices

2.2.1. Perpendicular dryness index (PDI)

The perpendicular distance (EF) in the NIR-Red space (refer to Figure 4), known as PDI, indicates dryness conditions and can be expressed as:
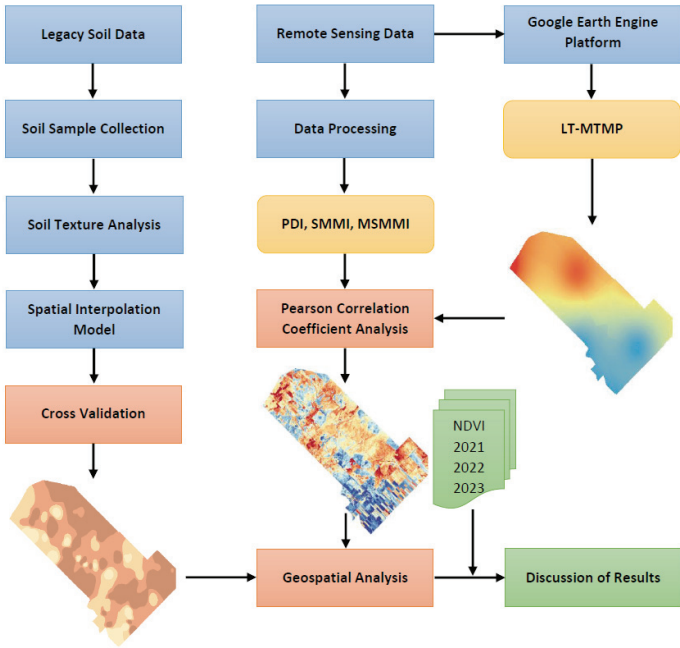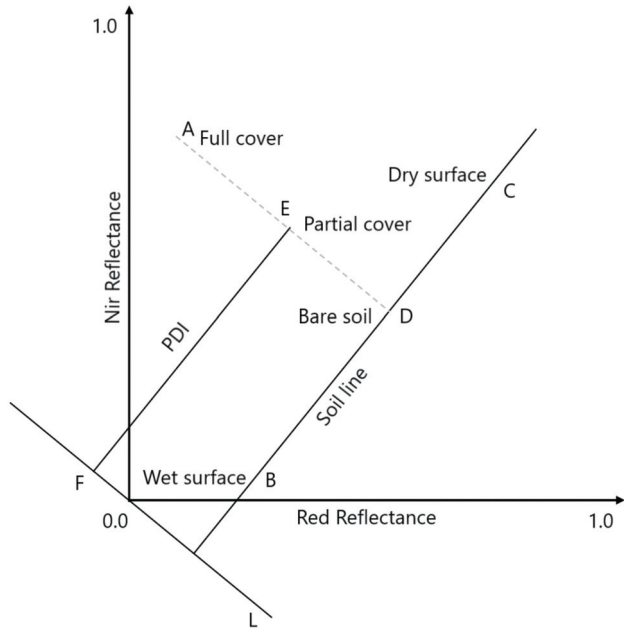

Fig. 3. Flowchart of methodology

Fig. 4. Sketch map of PDI

$$PDI = (R_{Red} + MR_{NIR})/\sqrt{1 + M^2}$$

The reflectance values of the Red and NIR bands are represented by R_{Red} and R_{NIR}, respectively. The variable M denotes the slope of the soil line BC, with B indicating the wet surface and C the dry surface. By analyzing the distribution of soil pixels in the NIR-Red space, we observe that the pixels forming the soil line are generally positioned at the bottom of the scatter plot, specifically where the lowest NIR reflectance value aligns with each red reflectance value (Yue et al., 2021). As a result, the value of M was automatically determined to be (0.9).

4

2.2.2. Soil moisture monitoring index (SMMI)

The distance from a point located at the origin O to the origin O itself is zero (0,0) in the NIR-Red space (Figure 5). An object's soil moisture content is inversely related to its distance from the origin O; specifically, the higher the soil moisture content of an object with a particular reflective capacity, the closer it is to the origin O (Liu et al., 2017; Liu et al., 2021). We employed the distance OE, known as SMMI, to evaluate the soil moisture status in the NIR-Red space, which can be calculated using the following equation:

A higher SMMI value suggests that point E is farther from point B, indicating reduced soil moisture, with A indicating full cover, B representing the wet surface, C signifying the dry surface, D denoting bare soil, and E illustrating partial cover as shown in the figure below.

2.2.3. Modified soil moisture monitoring index (MSMMI)

Since the SMMI does not consider the effects of vegetation coverage, researchers developed the MSMMI, which is based on fractional vegetation cover (FVC) and can be expressed as:

$$MSMMI = \frac{\sqrt{(R_{Red} - FVC \times R_{v,Red})^2 (R_{NIR} - FVC \times R_{v,NIR})^2}}{1 - FVC}$$

With

$$FVC = 1 - \left(\frac{NDVI_{max} - NDVI}{NDVI_{max} - NDVI_{min}}\right)^{0.6715}$$

where, $R_{v, Red}$ and $R_{v, NIR}$ refer to the reflectance of pure vegetation pixels in the Red and NIR bands, respectively. $NDVI_{max}$ and $NDVI_{min}$ denote the maximum and minimum values of NDVI, respectively (Liu et al., 2021; Yue et al., 2021).
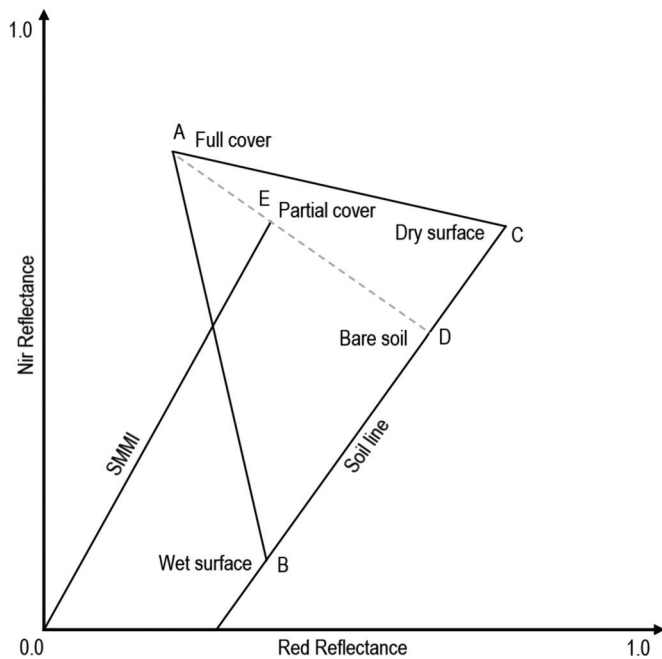

Fig. 5. Sketch map of SMMI

2.3. Precipitation

The processes of chemical and physical weathering in soil are primarily influenced by the climate (Kalaiselvi et al., 2024). Precipitation impacts soil by influencing vegetation growth and altering soil nutrient inputs (Li et al., 2023). Numerous studies have indicated that plant development is contingent upon soil moisture and precipitation (Papagiannopoulou et al., 2017; Joiner et al., 2018). While precipitation offers only indirect insights into the conditions of surface water, vegetation directly uses the moisture in the soil (Yang et al., 2015).

The LT-MTMP for a five-year period (2019–2023) was calculated using data obtained from the ERA5 dataset, which is produced by the Copernicus Climate Change Service (C3S) (Website:https://cds.climate.copernicus.eu). ERA5 is a global reanalysis dataset that provides hourly estimates of various atmospheric, land, and oceanic climate variables (Muñoz-Sabater et al., 2021). The LT-MTMP was derived by first extracting monthly precipitation data for the study area from the ERA5 dataset and then averaging the monthly values over the five-year period to obtain the long-term mean precipitation for each month. The extracted data was processed using the GEE platform, a cloud-based geospatial analysis tool that enables efficient handling of large-scale datasets (Ghosh et al., 2022). In GEE, the ERA5 precipitation data was clipped to the spatial extent of the study area, and temporal aggregation functions were applied to compute the long-term mean monthly precipitation values. This platform was chosen for its ability to handle large datasets efficiently and perform geospatial operations at scale.

To further refine the dataset, the original ERA5 precipitation data was spatially resampled using the Geo-statistical Analyst tool within ArcGIS Pro. This step was performed to improve the quality and spatial resolution of the dataset and to ensure alignment with the raster grids of drought indices used in subsequent analyses. This ensured that the precipitation data was compatible with the spatial resolution and grid structure of the drought indices, facilitating accurate spatial analysis and integration.

3. Results

The Fig. 6 demonstrates that the soil dryness status, as represented by the PDI and SMMI maps, appears visually similar. Although the dryness conditions for the drought indices were similar, the results were less severe than those from the MSMMI index. The PDI and SMMI indices show that humidity levels are increasing in the southern regions and at a low rate in the northern regions, while the central region is experiencing a clear level of drought. The MSMMI index generally indicates higher levels of drought, with some humidity present in the southern region and very weakly in the central region.

The Fig. 7 shows the monthly precipitation means for the study area over five years (2019, 2020, 2021, 2022, and 2023). It is noted that the lowest precipitation rates occur in July and August for all years. The figure also illustrates the variation in
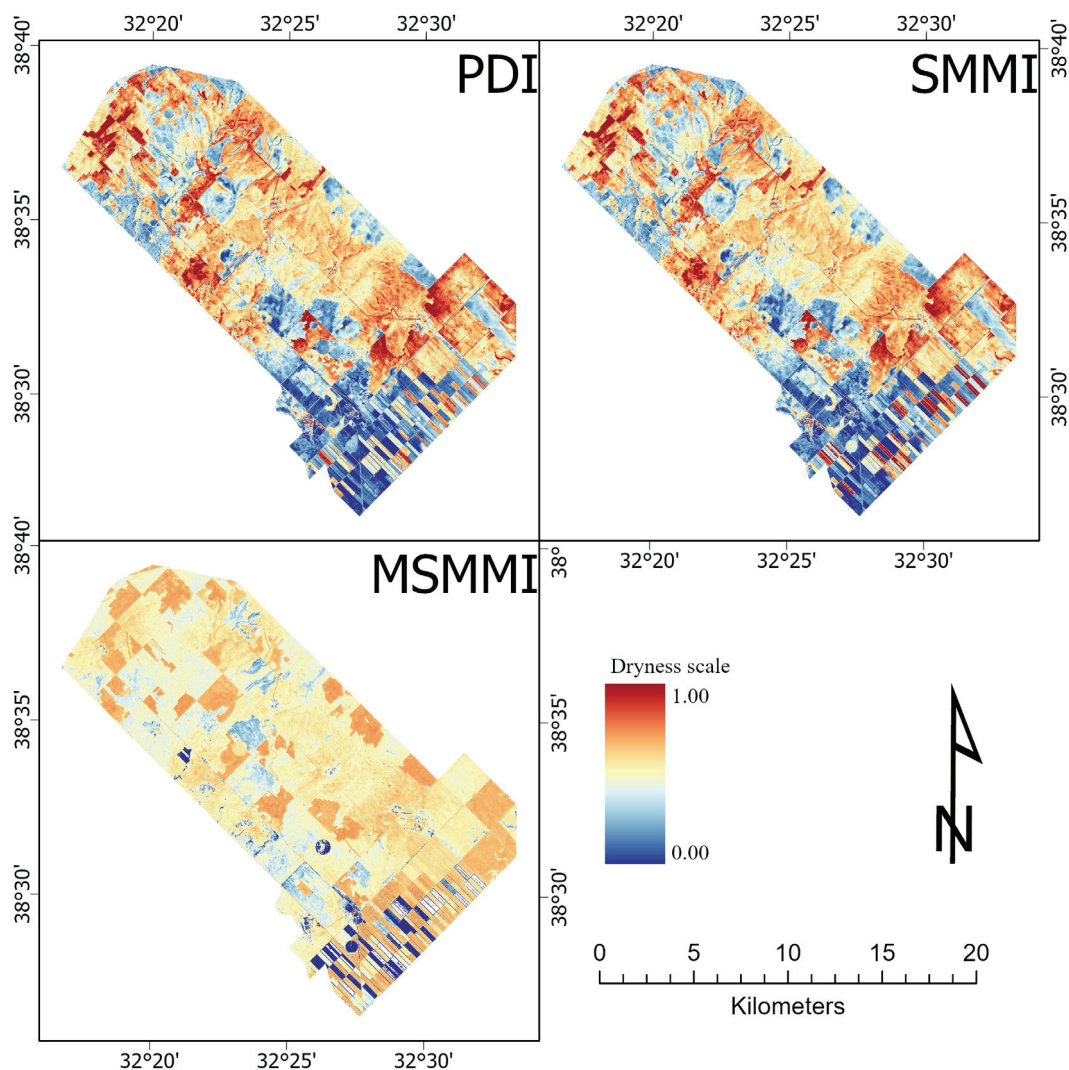
5

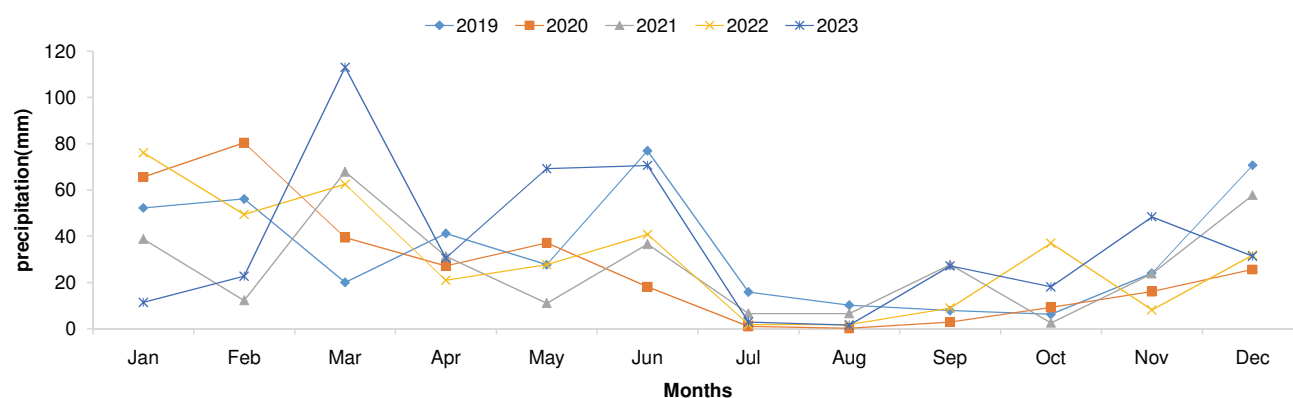**Fig. 6.** The soil moisture map by PDI, SMMI, and MSMMI indicators

Fig. 7. Monthly precipitation means for five years (2019–2023)

monthly precipitation means throughout the year for all years, except for March 2023, when the precipitation mean reached 113.07 mm, the highest monthly precipitation mean compared to the other years.

Using the Google Earth Engine platform and precipitation data obtained from the ERA5 dataset for the period 2019–2023, we simulated the mean total monthly precipitation for the study area during this period, as shown in (Fig. 8). Each pixel
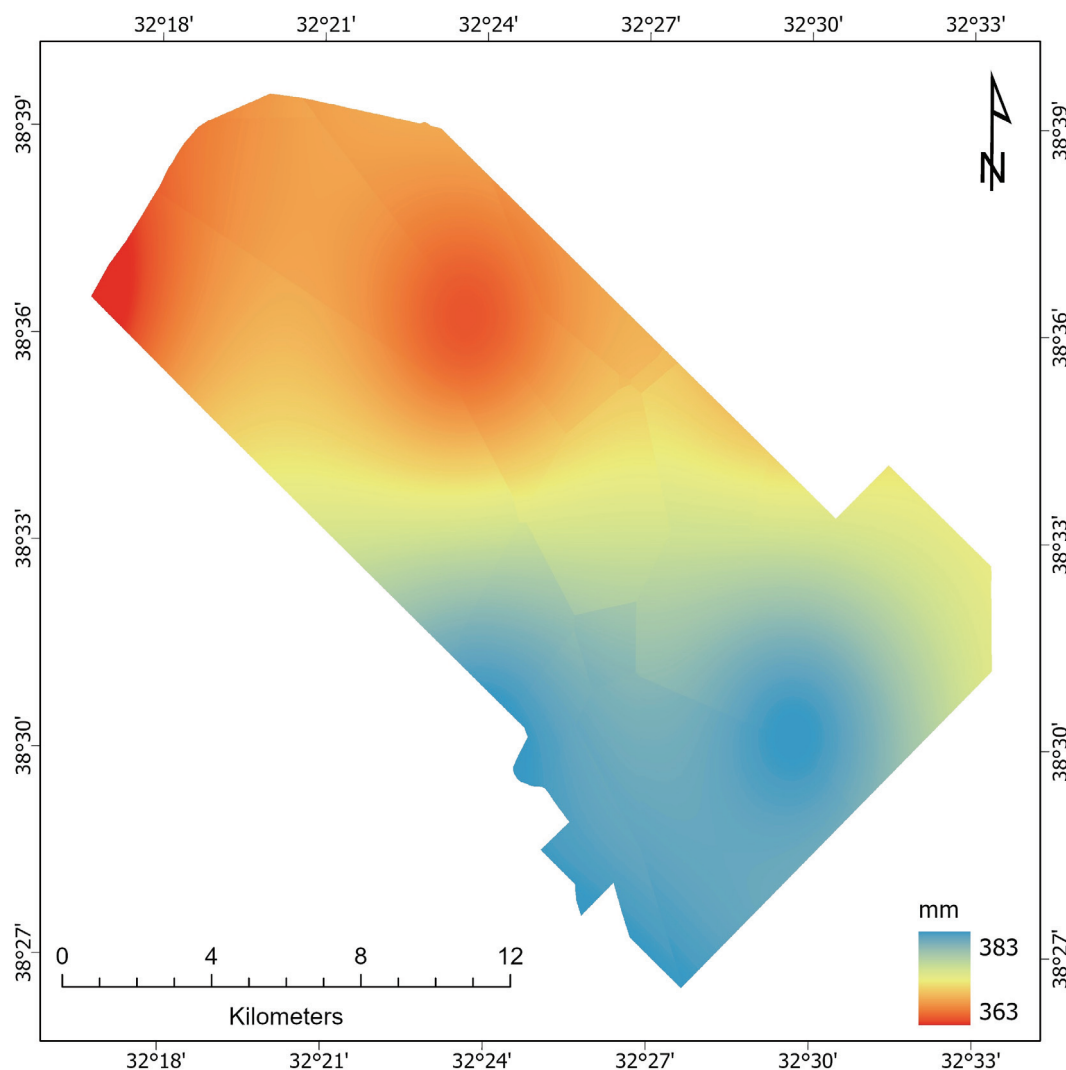
6

Fig. 8. LT-MTMP map (2019–2023)

on this map represents a distinct value simulating the mean total monthly precipitation that occurred over five years, providing a comprehensive view of the geographical distribution of precipitation in the enterprise. The map indicates that the southern region received the highest precipitation, which gradually decreased toward the north. It is also noted that the lowest amount of precipitation was found in the north-eastern part of the enterprise. The highest value was 383 mm, while the lowest was 363 mm. This narrow range between the highest and lowest precipitation values may be attributed to the relatively small area of the enterprise and its limited topographical diversity.

The Figs. 9, 10, and 11 show that all drought indices have a negative linear relationship with LT-MTMP. This indicates that an increase in LT-MTMP corresponds to a decrease in the drought index. Consequently, as the index value approaches zero, there is an increase in soil moisture. The scatter plots indicate that the highest negative PCC value was –0.69 at p-value < 0.01 between the PDI index and LT-MTMP. In contrast, the lowest PCC value was –0.24 at p-value < 0.05 between MSMMI

and LT-MTMP. Additionally, the PCC value of SMMI and LT-MTMP was –0.66 at p-value < 0.01.

The deviation of a few scattered samples from the fitting line, especially with the MSMMI index, is due mainly to their location in areas with high soil moisture. This indicates that remote sensing techniques can effectively reflect the spatial variation in surface soil moisture (Abdikan et al., 2023).

The Fig. 12 presents a spatial map of soil texture classes according to the USDA system (Bouyoucos, 1951) for the Gozlu agricultural enterprise, interpolated by the IDW spatial interpolation model with a mean error of 0.0049, as determined by cross-validation. The study area comprises four distinct soil texture classes. The spatial distribution shows that L and SCL textures extend north to south. In contrast, SL and CL textures are distributed as zones throughout most of the study area, particularly in the northwest and southwest. The results showed the SCL textures occupied the most significant percentage of the enterprise at 38.75%, while the SL textures had the smallest percentage at 7.41%. CL and L textures accounted for 21.31% and 32.52%, respectively.
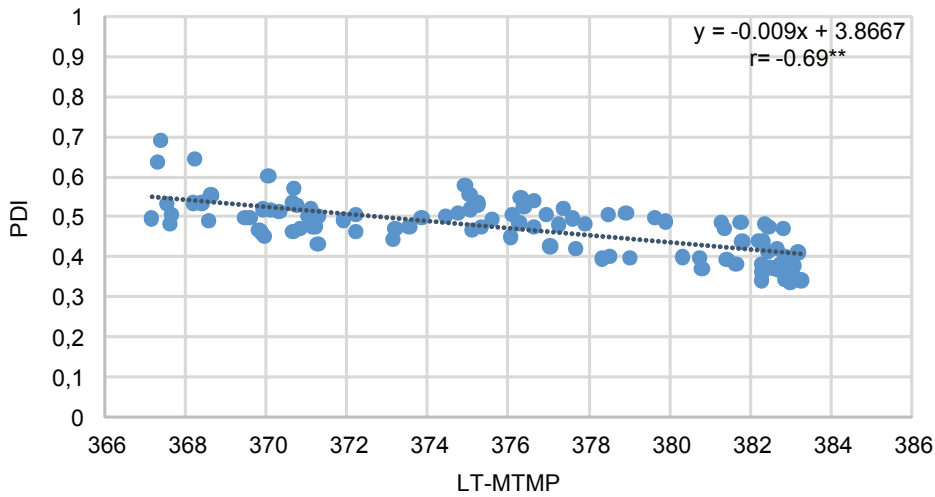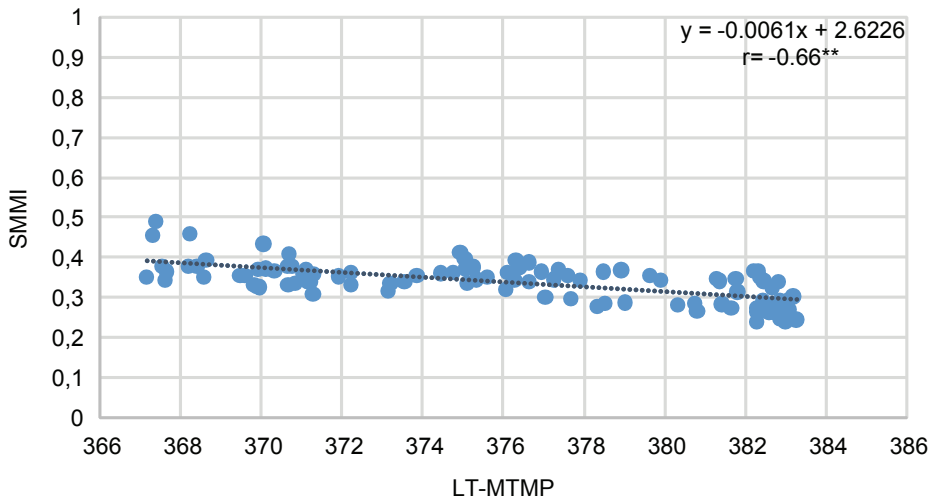
7

Fig. 9. PDI and LT-MTMP relationship

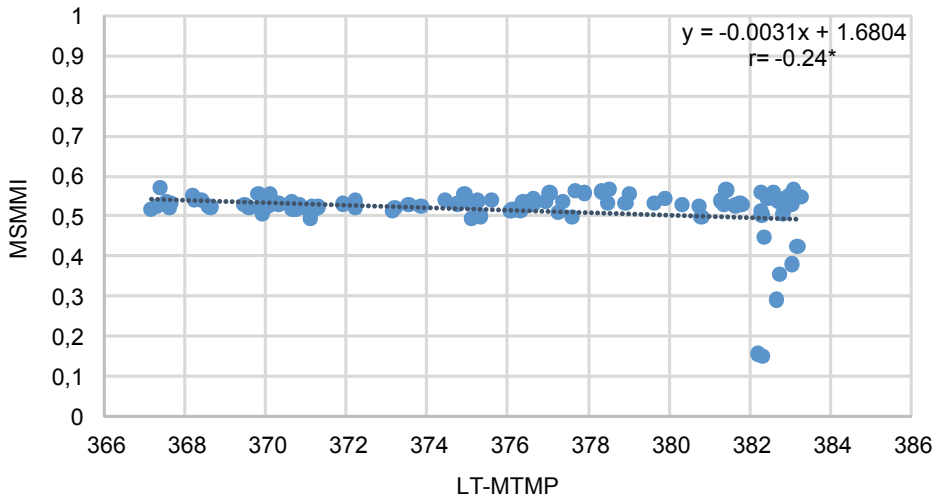**Fig. 10.** SMMI and LT-MTMP relationship

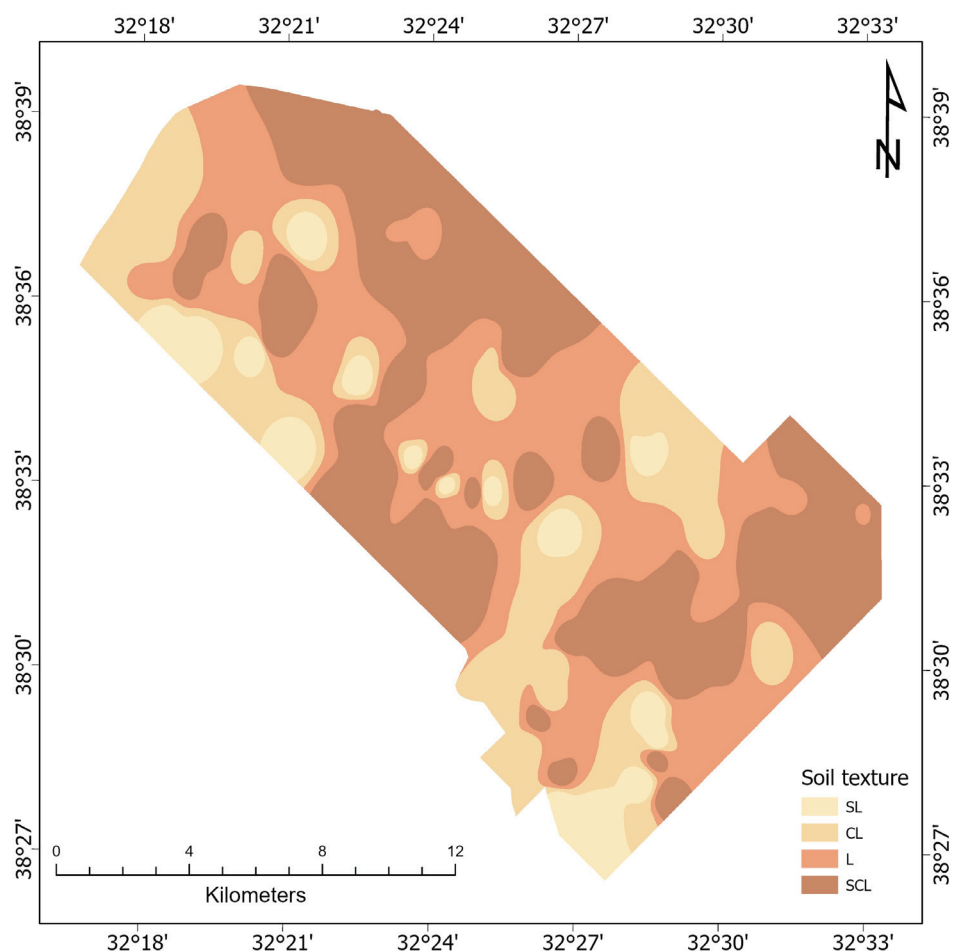**Fig. 11.** MSMMI and LT-MTMP relationship

Fig. 12. The soil texture map

4. Discussion

The soil moisture estimation results for the three indices showed that the NIR-Red feature space effectively reflects the dry and wet situations of the soil surface (Amani et al., 2016; Chen et al., 2017). Additionally, PDI proved to be more appropriate for observing soil moisture in bare soil or areas with little to no vegetation. This aligns with the findings of (Zhu et al., 2010; Wang et al., 2020). The outcomes of our paper indicated that the highest correlation was found between the PDI and SMMI drought indices and the LT-MTMP, with values of r = –0.69 and r = –0.66, respectively, and both indices are suitable for monitoring topsoil moisture; this is consistent with what was reached by (Liu et al., 2017). (Liu et al., 2018) introduced the MSMMI index, which is derived from SMMI index and FVC, and found that its monitoring accuracy matched that of MPDI index in semi-arid regions. Accordingly, one of the two dryness indices mentioned was selected for testing on the Gozlu agricultural enterprise.

Although the MSMMI accounted for vegetation, and the fields of the enterprise were partially cultivated with plants in September, the index indicated low biomass due to the arid ecosystem in the study area. This could explain why SMMI and PDI might have outperformed MSMMI in terms of results. These circumstances also make it clearer why locations with bare soil or little plant cover are better suited for using SMMI and PDI for estimating soil moisture. This conclusion aligns with the findings of (Yue et al., 2021).

Table 2 shows that the SL soil texture had the highest percentage of area classified as wet class within the dryness levels, amounting to 32.45%. Although this soil texture contains sand fractions, the vegetation cover was dominant in the SL soil texture for the years 2021, 2022, and 2023. This finding is consistent with the outcomes of a study conducted in the Tibetan Plateau, which integrated the NDVI with soil type to explore the potential impact of climate change on ecosystems (Jiang et al., 2020). In

Table 2

Percentage of dryness levels of PDI for soil texture classes

PDI	Soil texture classes (USDA system)			
	SL	SCL	L	CL
Very Wet	0.00	0.00	0.00	0.00
Wet	32.45	8.46	11.69	19.75
Normal	66.27	90.64	88.13	77.86
Dryness	1.26	0.88	1.66	2.37
Very Dryness	0.00	0.01	0.00	0.00

9

addition, cultivated fields have a higher percentage of organic matter, which results from addition of this matter or decomposition of plant residues. Consequently, organic matter increases the soil's water retention (Amooh and Bonsu, 2015). The dryness level (wet class) of the CL soil texture reached 19.75% of the total area of this soil texture, which was higher than that of the L and SCL soil textures. This is due to the presence of clay fractions, which are superior in retaining moisture compared to other soil texture fractions. The small particle size of those less than 0.002 mm, which has a higher ability to hold water between its particles, contributes to this effect. This outcomes is consistent with the study of (Renne et al., 2019), who indicated that fine-textured soils have a higher ability to retain water compared to the coarse-textured soils. As for the soil textures, L and SCL, the percentage of area classified as wet class reached 11.69% and 8.46%, respectively, with the SCL soil texture having the lowest percentage compared to the other soil textures. This is due to the percentage of sand fractions in this soil textures type and the size of sand particles, whose diameters range between 0.05 mm and 2.0 mm. It is scientifically established the soils with different textures exhibit varying characteristics, such as grain size, void ratio, and permeability, which can significantly influence the resistance and resilience of vegetation to drought stress (Jiang et al., 2020). These outcomes are consistent with those obtained by (Rajput et al., 2024).

5.   Conclusions

This study calculated three drought indices PDI, SMMI, and MSMMI which utilize the NIR-Red feature area. Their relationship with LT-MTMP (2019–2023) was analyzed within study area (Gozlu agricultural enterprise) located in central Anatolia plateau, Turkey. The outcomes showed that the highest negative correlation among the three indices was for the PDI, which reached r = –0.69 with LT-MTMP. Four soil texture classes SL, CL, L, and SCL were identified in the study area through laboratory analysis. Geospatial techniques were then used to spatially classify each soil texture class into five levels of dryness based on the PDI. The results showed that the (wet class) dryness level had the highest area percentage (32.45%) with the SL soil texture, despite its sand fractions content. This was followed by CL and L soil textures, with 19.75% and 11.69%, respectively. The SCL soil texture had the lowest area percentage of 'wet' dryness level at 8.46%. Additionally, the investigation revealed that the area percentage of SL soil texture covers only 7.41% of the total study area, making it the smallest area compared to the area of other soil texture types. Moreover, the vast majority of this area is used for growing vegetables, which means that there are organic matter additions through human intervention or decaying plant remains and irrigation processes, which led to partially irregular results.

The outcomes of this study showed that increasing the clay particle content improves the soil's water retention capacity, while increasing the sand particle content has the opposite effect under rainfed farming conditions and low organic matter content. Therefore, the soil's ability to retain water varies depending on its texture and other features. In addition, the changes in soil texture are apparent only on long time scales, spanning decades or even centuries. Therefore, understanding the spatial distribution and storage capacity of soil moisture is crucial. In this context, such analyses may provide a deeper comprehending of the potential impact of drought on vegetation, considering soil characteristics. However, factors beyond soil texture concept, such as hydrological properties and soil organic matter, should be considered, as they can significantly influence water stress levels and, consequently, water availability for plants.

Conflict of interest

The authors declare that no potential conflicts of interest were reported. This research did not involve human or animal subjects.

Author contribution

The first author conceptualized the research idea, designed the methodology, and performed the correlation analysis under the supervision of Assoc. Prof. Dr. Mert Dedeoğlu. The first author also conducted the field sampling and laboratory analysis to determine soil texture and developed the geospatial interpolation map. Authors contributed to data analysis, interpretation of results, and validation of findings. The manuscript, including the introduction, discussion, and final version, was collaboratively written and revised by authors.

References

Abdikan, S., Sekertekin, A., Madenoglu, S., Ozcan, H., Peker, M., Pinar, M.O., Koc, A., Akgul, S., Secmen, H., Kececi, M., Tuncay, T., Balik Sanli, F., 2023. Surface soil moisture estimation from multi-frequency SAR images using ANN and experimental data on a semi-arid environment region in Konya, Turkey. Soil and Tillage Research 228, 105646. https://doi.org/https://doi.org/10.1016/j.still.2023.105646

Amani, M., Parsian, S., MirMazloumi, S.M., Aieneh, O., 2016. Two new soil moisture indices based on the NIR-red triangle space of Landsat-8 data. International Journal of Applied Earth Observation and Geoinformation 50, 176–186. https://doi.org/https://doi.org/10.1016/j.jag.2016.03.018

Amooh, M.K., Bonsu, M., 2015. Effects of soil texture and organic matter on evaporative loss of soil moisture. Journal of Global Agriculture and Ecology 3, 152–161.

Bouyoucos, G.J., 1951. A recalibration of the hydrometer method for making mechanical analysis of soils. Agronomy Journal 43(9), 434–438.

Chen, N., He, Y., Zhang, X., 2017. Nir-red spectra-based disaggregation of smap soil moisture to 250 m resolution based on oznet in southeastern australia. Remote Sensing 9(1), 51. https://doi.org/https://doi.org/10.3390/rs9010051

Chen, N., Li, J., Zhang, X., 2015. Quantitative evaluation of observation capability of GF-1 wide field of view sensors for soil moisture inversion. Journal of Applied Remote Sensing 9(1), 097097–097097. https://doi.org/https://doi.org/10.1117/1.JRS.9.097097

ÇÜ, TİGEM. 1998. Gözlü Tarım İşletmesi Topraklarının Detaylı Toprak Etüd ve Haritalanması. (in Turkish)

Dutta, D., Kundu, A., Patel, N., Saha, S., Siddiqui, A., 2015. Assessment of agricultural drought in Rajasthan (India) using remote sensing derived Vegetation Condition Index (VCI) and Standardized Precipitation Index (SPI). The Egyptian Journal of Remote Sensing and Space Science 18(1), 53–63. https://doi.org/https://doi.org/10.1016/j.ejrs.2015.03.006

Ghosh, S., Kumar, D., Kumari, R., 2022. Cloud-based large-scale data retrieval, mapping, and analysis for land monitoring applications with google earth engine (GEE). Environmental Challenges 9, 100605. https://doi.org/https://doi.org/10.1016/j.envc.2022.100605

Gümüş, K.A., Balçık, F.B., Esetlili, T., Kahya, C., 2023. Monitoring drought dynamics using remote sensing-based combined drought index in Ergene Basin, Türkiye. Open Geosciences 15(1). https://doi.org/https://doi.org/10.1515/geo-2022-0594

Hao, L., Zhang, X., Liu, S., 2012. Risk assessment to China's agricultural drought disaster in county unit. Natural hazards 61, 785–801. https://doi.org/https://doi.org/10.1007/s11069-011-0066-4

Jiang, L., Bao, A., Guo, H., Ndayisaba, F., 2017. Vegetation dynamics and responses to climate change and human activities in Central Asia. Science of Total Environment 599, 967–980. https://doi.org/https://doi.org/10.1016/j.scitotenv.2017.05.012

Jiang, P., Ding, W., Yuan, Y., Ye, W., 2020. Diverse response of vegetation growth to multi-time-scale drought under different soil textures in China's pastoral areas. Journal of Environmental Management 274, 110992. https://doi.org/https://doi.org/10.1016/j.jenvman.2020.110992

Joiner, J., Yoshida, Y., Anderson, M., Holmes, T., Hain, C., Reichle, R., Koster, R., Middleton, E., Zeng, F.W., 2018. Global relationships among traditional reflectance vegetation indices (NDVI and NDII), evapotranspiration (ET), and soil moisture variability on weekly timescales. Remote Sensing of Environment 219, 339–352. https://doi.org/https://doi.org/10.1016/j.rse.2018.10.020

Kalaiselvi, B., Chakraborty, R., Dharumarajan, S., Kumar, K.A., Hegde, R., 2024. Spatial prediction of soil organic carbon and its stocks using digital soil mapping approach. In *Remote Sensing of Soils*. Elsevier, pp. 411–428. https://doi.org/https://doi.org/10.1016/B978-0-443-18773-5.00003-X

Kang, J., Jin, R., Li, X., Ma, C., Qin, J., Zhang, Y., 2017. High spatio-temporal resolution mapping of soil moisture by integrating wireless sensor network observations and MODIS apparent thermal inertia in the Babao River Basin, China. Remote Sensing of Environment 191, 232–245. https://doi.org/https://doi.org/10.1016/j.rse.2017.01.027

Kaya, F., Meşe, O., Başayiğit, L., 2022. Geostatistical-based mapping of topsoil texture in Fluvisols and Vertisols around Lake of Manyas. Intercontinental Geoinformation Days 4, 68–73.

Kimura, R., Moriyama, M., Saylan, L., 2023. Monitoring of Recent Aridification in Türkiye Using MODIS Satellite Data from 2000 to 2021. Scientific Online Letters on the Atmosphere 19, 94–100. https://doi.org/https://doi.org/10.2151/sola.2023-013

Li, Y., Wang, X., Chen, Y., Gong, X., Yao, C., Cao, W., Lian, J., 2023. Application of predictor variables to support regression kriging for the spatial distribution of soil organic carbon stocks in native temperate grasslands. Journal of Soils and Sediments 23(2), 700–717. https://doi.org/https://doi.org/10.1007/s11368-022-03370-1

Liu, Y., Li, Y., Lu, Y., Yue, H., 2018. Comparison and application of MPDI and MSMMI for drought monitoring in desert mining area. IOP Conference Series: Earth and Environmental Science, https://doi.org/https://doi.org/10.1088/1755-1315/146/1/012001

Liu, Y., Qian, J., Yue, H., 2020. Combined Sentinel-1A with Sentinel-2A to estimate soil moisture in farmland. IEEE Journal of Selected Topics in Applied Earth Observations and Remote Sensing 14, 1292–1310. https://doi.org/https://doi.org/10.1109/JSTARS.2020.3043628

Liu, Y., Qian, J., Yue, H., 2021. Comprehensive evaluation of Sentinel-2 red edge and shortwave-infrared bands to estimate soil moisture. IEEE Journal of Selected Topics in Applied Earth Observations and Remote Sensing 14, 7448–7465. https://doi.org/https://doi.org/10.1109/JSTARS.2021.3098513

Liu, Y., Wu, L., Ma, B., 2013. Remote sensing monitoring of soil moisture on the basis of TM/ETM+ spectral space. Journal of China University of Mining and Technology 42(2), 296–301.

Liu, Y., Wu, L., Yue, H., 2015. Biparabolic NDVI-Ts space and soil moisture remote sensing in an arid and semi arid area. Canadian Journal of Remote Sensing 41(3), 159–169. https://doi.org/https://doi.org/10.1080/07038992.2015.1065705

Liu, Y., Yue, H., 2018. The temperature vegetation dryness index (TVDI) based on Bi-parabolic NDVI-Ts space and gradient-based structural similarity (GSSIM) for long-term drought assessment across Shaanxi province, China (2000–2016). Remote Sensing 10(6), 959. https://doi.org/https://doi.org/10.3390/rs10060959

Liu, Y., Yue, H., Wang, H., Zhang, W., 2017. Comparison of SMMI, PDI and its applications in Shendong mining area. IOP Conference Series: Earth and Environmental Science, https://doi.org/https://doi.org/10.1088/1755-1315/57/1/012025

Mishra, A.K., Singh, V.P., 2010. A review of drought concepts. Journal of hydrology 391(1–2), 202–216. https://doi.org/https://doi.org/10.1016/j.jhydrol.2010.07.012

Muñoz-Sabater, J., Dutra, E., Agustí-Panareda, A., Albergel, C., Arduini, G., Balsamo, G., Boussetta, S., Choulga, M., Harrigan, S., Hersbach, H., Martens, B., Miralles, D.G., Piles, M., Rodríguez-Fernández, N.J., Zsoter, E., Buontempo, C., Thépaut, J.N., 2021. ERA5-Land: a state-of-the-art global reanalysis dataset for land applications. Earth System Science Data 13(9), 4349–4383. https://doi.org/10.5194/essd-13-4349-2021

Özen, D., Kocakaya, A., Ozbeyaz, C., 2021. Estimating relationship between live body weight and type traits at weaning and six months of age in Bafra lambs using canonical correlation analysis. Journal of Animal and Plant Sciences 31(2). https://doi.org/http://doi.org/10.36899/japs.2021.2.0226

Papagiannopoulou, C., Miralles, D., Dorigo, W.A., Verhoest, N., Depoorter, M., Waegeman, W., 2017. Vegetation anomalies caused by antecedent precipitation in most of the world. Environmental Research Letters 12(7), 074016. https://doi.org/http://doi.org/10.1088/1748-9326/aa7145

Quiring, S.M., Ganesh, S., 2010. Evaluating the utility of the Vegetation Condition Index (VCI) for monitoring meteorological drought in Texas. Agricultural and Forest Meteorology 150(3), 330–339. https://doi.org/https://doi.org/10.1016/j.agrformet.2009.11.015

Rajput, U., Sharma, S., Swami, D., Joshi, N., 2024. Rapid assessment of soil–water retention using soil texture-based models. Environmental Earth Sciences 83(16), 1–15. https://doi.org/https://doi.org/10.1007/s12665-024-11755-3

Renne, R.R., Bradford, J.B., Burke, I.C., Lauenroth, W.K., 2019. Soil texture and precipitation seasonality influence plant community structure in North American temperate shrub steppe. Ecology 100(11), e02824. https://doi.org/https://doi.org/10.1002/ecy.2824

Sawada, Y., 2018. Quantifying drought propagation from soil moisture to vegetation dynamics using a newly developed ecohydrological land reanalysis. Remote Sensing 10(8), 1197. https://doi.org/https://doi.org/10.3390/rs10081197

Singh, R.P., Roy, S., Kogan, F., 2003. Vegetation and temperature condition indices from NOAA AVHRR data for drought monitoring over India. International Journal of Remote Sensing 24(22), 4393–4402. https://doi.org/https://doi.org/10.1080/0143116031000084323

Wang, H., He, N., Zhao, R., Ma, X., 2020. Soil water content monitoring using joint application of PDI and TVDI drought indices. Remote Sensing Letters 11(5), 455–464. https://doi.org/https://doi.org/10.1080/2150704X.2020.1730469

Website:https://cds.climate.copernicus.eu.

Yang, C., Wang, G.G., Wang, M.L., 2015. A study on the sustainability of Chinese pasturing and semi-pasturing grassland based on ecological footprint model. Advanced Materials Research 1073, 2578–2582. https://doi.org/https://doi.org/10.4028/www.scientific.net/AMR.1073-1076.2578

Yue, H., Liu, Y., Qian, J., 2021. Comparative assessment of drought monitoring index susceptibility using geospatial techniques. Environmental Science and Pollution Research 28, 38880–38900. https://doi.org/https://doi.org/10.1007/s11356-021-13275-0

Zhang, J., Zhang, Q., Bao, A., Wang, Y., 2019. A New Remote Sensing Dryness Index Based on the Near-Infrared and Red Spectral Space. Remote Sensing 11(4), 456. https://doi.org/https://doi.org/10.3390/rs11040456

Zhang, X., Chen, N., 2016. Reconstruction of GF-1 soil moisture observation based on satellite and in situ sensor collaboration under full cloud contamination. IEEE Transactions on Geoscience and Remote Sensing 54(9), 5185–5202. https://doi.org/https://doi.org/10.1109/TGRS.2016.2558109

Zhu, C., Wei, Y., Zhu, F., Lu, W., Fang, Z., Li, Z., Pan, J., 2022. Digital mapping of soil organic carbon based on machine learning and regression kriging. Sensors 22(22), 8997. https://doi.org/https://doi.org/10.3390/s22228997

Zhu, L., Liu, J., Zhang, Y., Wang, M., 2010. Application of FY-3A/MERSI satellite data to drought monitoring in north China. Journal of Remote Sensing 14(5), 1004–1016.